Tomographic reconstruction of weak, replicated index structures embedded in a volume

Amy C. Sullivan[1,*] and Robert R. McLeod[2]

[1]*Department of Physics, University of Colorado, Campus Box 390, Boulder, CO 80309*
[2]*Department of Electrical and Computer Engineering, University of Colorado, Campus Box 425, Boulder, CO 80309*
**Corresponding author: amy.sullivan@colorado.edu*

Abstract: Measurements of weak, embedded index structures are important for material characterization of photopolymers, glass and other optical materials as well as for characterization of fabricated structures such as waveguides. We demonstrate an optical diffraction tomography system capable of measuring deeply-buried, weak, fabricated index structures written in a homogeneous volume. High-fidelity cross sections of these weak index structures are constructed by replicating the structure to be measured to form a diffraction grating. The coherent addition of scattering from each of these objects increases the sensitivity of the imaging system. Measurements are made in the far field, without the use of lenses, eliminating phase aberration errors through thick volumes.

OCIS codes: (110.6960) Tomography; (050.1950) Diffraction gratings; (160.5470) Polymers.

References and links

1. M. Schnoes, B. Ihas, A. Hill, L. Dhar, D. Michaels, S. Setthachayanon, G. Schomberger, W. L. Wilson, "Holographic data storage media for practical systems," Proc. SPIE **5005**, 29–37 (2003).
2. R. A. Waldman, R. T. Ingwall, P. K. Dhal, M. G. Horner, E. S. Kolb, H-Y. S. Li, R. A. Minns, and H. G. Schild, "Cationic ring-opening photopolymerization methods for holography," Proc. SPIE **2689**, 127–141 (1996).
3. W. S. Colburn and K. A. Haines, ''Volume hologram formation in photopolymer materials,'' Appl. Opt. **10**, 1636–1641 (1971).
4. G. Zhao and P. Mouroulis, ''Diffusion model of hologram formation in dry photopolymer materials,'' J. Mod. Opt. **41**, 1929–1939 (1994).
5. V. L. Colvin, R. G. Larson, A. L. Harris, and M. L. Schilling, "Quantitative model of volume hologram formation in photopolymers," J. Appl. Phys. **81**, 5913–5923 (1997).
6. J. T. Sheridan and J. R. Lawrence, "Nonlocal-response diffusion model of holographic recording in photopolymer," J. Opt. Soc. Am. A **17**, 1108–1114 (2000).
7. R. R. McLeod, A. J. Daiber, M. E. McDonald, T. L. Robertson, T. Slagle, S. L. Sochava, and L. Hesselink, "Microholographic multilayer optical disk data storage," Appl. Opt. **44**, 3197–3207 (2005).
8. B. L. Booth, "Low loss channel waveguides in polymers," J. Lightwave Technol. **7**, 1445–1453 (1989).
9. A. S. Kewitsch and A. Yariv, "Self-focusing and self-trapping of optical beams upon photopolymerization," Opt. Lett. **21**, 24–26 (1996).
10. M. Yonemura, A. Kawasaki, S. Kato, and M. Kagami, "Polymer waveguide module for visible wavelength division multiplexing plastic optical fiber communication," Opt. Lett. **30**, 2206–2208 (2005).
11. A. C. Sullivan, M. W. Grabowski, R. R. McLeod, "Three-dimensional direct-write lithography into photopolymer," Appl. Opt., **46**, 295–301 (2007).
12. K. M. Davis, K. Miura, N. Sugimoto, and K. Hirao, "Writing waveguides in glass with a femtosecond laser," Opt. Lett. **21**, 1729–1731 (1996).
13. M. Will, S. Nolte, B. N. Chichkov, and A. Tünnermann, "Optical properties of waveguides fabricated in fused silica by femtosecond laser pulses," Appl. Opt. **41**, 4360–4364 (2002).
14. A. M. Kowalevicz, V. Sharma, E. P. Ippen, J. G. Fujimoto, and K. Minoshima, "Three-dimensional photonic devices fabricated in glass by use of a femtosecond laser oscillator," Opt. Lett. **30**, 1060–1062 (2005).
15. M. Pluta, *Advanced Light Microscopy Vol. 2. Specialized Methods*, (Elsevier, NY 1989), pp. 146–197.
16. C. J. Cogswell and C. J. R. Sheppard, "Confocal differential interference contrast (DIC) microscopy: including a theoretical analysis of conventional and confocal DIC imaging," J. Microsc. **165**, 81–101 (1992).

#86306 - $15.00 USD Received 9 Aug 2007; revised 5 Oct 2007; accepted 10 Oct 2007; published 12 Oct 2007

17. S. V. King, Department of Electrical and Computer Engineering, University of Colorado, Campus Box 425, Boulder, CO 80309, USA, A. Libertun, C. Preza, R. Piestun, and C. J. Cogswell are preparing a manuscript to be called "Quantitative phase microscopy through differential interference imaging."
18. C. J. R. Sheppard, D. M. Shotton, *Confocal laser scanning microscopy*, (BIOS Scientific, 1997).
19. T. Wilson, Y. Kawata, and S. Kawata, "Readout of three-dimensional optical memories," Opt. Lett. **21**, 1003–1005 (1996).
20. C. J. Cogswell, and J. W. O'Byrne, "High-resolution confocal transmission microscope, Part I: system design," Proc. SPIE **1660**, 503–511 (1992).
21. M. J. Booth, M. A. A. Neil, R. Juskaitis, T. Wilson, "Adaptive aberration correction in a confocal microscope," Proceedings of the National Academy of Sciences **99**, pp. 5788-5792 (2002).
22. M. M. Woolfson, *An introduction to X-ray crystallography*, ed. 2 (Cambridge University Press, 1997).
23. M. Born and E. Wolf, *Principles of Optics*, ed. 7 (Cambridge University Press, 1999).
24. A. C. Kak, M. Slaney, *Principles of Computerized Tomographic Imaging* (IEEE Press, 1988).
25. B. Chen and J. J. Stamnes, "Validity of diffraction tomography based on the first Born and the first Rytov approximations," Appl. Opt. **37**, 2996–3006 (1998).
26. R. T. Weverka, K. Wagner, R. R. Mcleod, K. Wu, and C. Garvin, "Low-Loss Acousto-Optic Photonic Switch," in *Acousto-Optic Signal Processing Theory and Implementation*, N. J. Berg and J. M. Pellegrino, eds. (Marcel Dekker, 1996), pp. 479 – 573.
27. S. X. Pan and A. C. Kak, "A computation study of reconstruction algorithms for Diffraction Tomography: Interpolation versus Filtered Backpropagation," IEEE Trans. Acoust. Speech Signal Process. **ASSP-31**, 1262–1275 (1983).
28. A. J. Devaney, "A Filtered Backpropagation Algorithm for Diffraction Tomography," Ultrasonic Imaging **4**, 336–350 (1982).
29. T. C. Wedberg and J. J. Stamnes, "Comparison of phase retrieval methods for optical diffraction tomography," Pure Appl. Opt. **4**, 39–54 (1995).
30. E. Wolf, "Determination of the amplitude and the phase of the scattered field by holography," J. Opt. Soc. Am. **60**, 18–20 (1970).
31. W. Singer, B. Dobler, H. Schreiber, K. Brenner, B. Messerschmidt, "Refractive-index measurement of gradient-index microlenses by diffraction tomography," Appl. Opt. **35**, 2167–2171 (1996).
32. InPhase Technologies, Tapestry Media, www.inphase-technologies.com.
33. C. J. Cogswell, N. I. Smith, K. G. Larkin, P. Hariharan, "Quantitative DIC microscopy using a geometric phase shifter," Proc. SPIE **2984**, 72–81 (1997).

1. Introduction

Quantitative, high-resolution images of weak index structures are important for a wide variety of applications. Accurate measurements of index changes in volume photopolymers are necessary for storage applications such as volume holographic storage and microholographic volume data storage [1–7]. Waveguides can also be written in photopolymers by mask lithography [8], using light from an embedded fiber to self-write a waveguide [9,10], or three-dimensional (3D) direct-write lithography [11]. Femtosecond writing in glass is also used to create embedded 3D waveguides and integrated optical circuits [12–14]. Quantitative measurements of these index structures written in photopolymers or glass are essential for design verification and development of materials response models. In this paper, we demonstrate an optical diffraction tomography system capable of quantitative imaging of weak index structures written in a 3D volume. This is accomplished by making many identical, equally-spaced copies of the object to be measured in order to increase the sensitivity of the imaging system. Many fabrication techniques, such as those described above, are capable of replicating many copies of the objects to be imaged. As we demonstrate in this paper, this allows for imaging weak index structures with a higher signal to noise ratio than traditional tomography.

Small or weak variations in the index can be very difficult to measure and the thickness of the samples makes imaging even more challenging. The total phase delay across small features can be much less than a single wavelength for a structure embedded millimeters deep in a glass or polymer sample. Differential Interference Contrast (DIC) microscopy is one technique for imaging these structures qualitatively and recent work has shown quantitative measurements of thin objects [15–17]. However, high-power objectives accumulate significant spherical aberrations when imaging through thick objects and have limited working distances. The objectives can be corrected for certain depths but cannot usually

#86306 - $15.00 USD Received 9 Aug 2007; revised 5 Oct 2007; accepted 10 Oct 2007; published 12 Oct 2007

image accurately over a wide range of depths, such as the 1 mm depth scanning required for many applications. Confocal scanning microscopy has excellent depth sectioning [18], but confocal reflection systems are not sensitive to the spatial frequencies of index structures written by a focused beam unless the numerical aperture (NA) of the confocal microscope is significantly higher than that of the NA of the writing lens [19]. Confocal transmission microscopy, on the other hand, is sensitive to objects with lower spatial frequencies, but is challenging to implement due to deflection and aberration of the transmitted spot [20,21]. All of the above techniques also have the same problem of accumulating significant spherical aberrations through very thick objects, which limits the working distance of the imaging system. Thick index objects can be sliced thinly in order to be imaged using one of these phase microscopy techniques; however, this may damage the object to be imaged.

Optical diffraction tomography solves many of these problems but has several limitations of its own. Diffraction tomography works by measuring the fields diffracted from an object at a number of incident probe beam angles and backpropagating the fields to reconstruct the scattering object. A collimated probe beam can be used, eliminating the need for high NA lenses and therefore eliminating phase aberration errors in the image. Also, by measuring the scattered field at a number of incident angles, the object is imaged in both the transverse and depth dimensions, allowing quantitative imaging of thick objects. Normally, diffraction tomography requires information about the phase of the scattered fields. This requirement significantly complicates both the experimental set up and the numerical reconstruction. Also, an object with a phase delay of much less than one wavelength diffracts light with an efficiency that is typically lower than the scattering background. Therefore, it is difficult to distinguish the signal from the noise. The tomography system reported here overcomes these two difficulties. First, for symmetric objects, phase information is not necessary for the reconstruction. The low signal-to-noise problem is addressed by duplicating the object of interest on a regular grid so that the scatter from each object adds coherently to the others, giving a stronger signal for the reconstruction. This method of duplicating the object of interest and reconstructing the object from discrete samples in the far field is similar to that used for x-ray diffraction measurements of crystals [22].

In Sec. 2, we review the fundamentals of optical diffraction tomography and the modifications made to the reconstruction algorithm for imaging diffraction gratings without phase. We then describe a 3D lithography system for fabricating a grid of identical weak, index structures with the required symmetry in Sec. 3. Details of the tomography system and the results and validation are presented in Sec. 4.

2. Optical diffraction tomography: theory

Optical diffraction tomography is used to reconstruct weak 3D index perturbations from a series of two-dimensional (2D) diffracted field measurements taken over a range of probe beam incident angles [23,24]. In the Born approximation, where the perturbation is small enough that the probe beam is essentially undepleted, the Fourier transform of the index perturbation is directly related to the Fourier transform of the scattered near field. Backpropagation of the scattered fields is accomplished by inverting the forward scattering problem. For many applications, the index perturbation is constant or slowly varying in one dimension and so the following derivation is concerned with imaging two dimensional cross sections of the index perturbation.

The problem of scattering off of inhomogeneous media is complex in full vector form, but a number of approximations can be made to simplify the problem for practical applications. It is common to assume that the scattering object varies slowly in space, i.e., it does not change significantly over distances on the order of the wavelength of the incident light. This simplification uncouples the different components of the electric field in the wave equation and simplifies the problem to the scalar case, which can be expressed in terms of the index of refraction, n, as

#86306 - $15.00 USD Received 9 Aug 2007; revised 5 Oct 2007; accepted 10 Oct 2007; published 12 Oct 2007

$$\left(\nabla^2 + k_0^2 n_0^2\right) E(x,z) = k_0^2 n_o^2 \left(1 - \frac{n^2(x,z)}{n_0^2}\right) E(x,z), \tag{1}$$

where $E(x,z)$ is the electric field of the probe beam, $n(x,z) = n_0 + \delta n(x,z)$ is the sum of the background index and the index perturbation, and $k_0 = 2\pi/\lambda_0$ is the wave number in free space. This simplification limits the applicable resolution of the tomography system to the order of a wavelength of the probe beam.

In the Born approximation, where the scattering is weak, the expression in the parentheses on the right side of Eq. (1) can be approximated by

$$1 - \frac{n^2(x,z)}{n_0^2} \approx -\frac{2\delta n(x,z)}{n_0}. \tag{2}$$

The field is then represented as a sum of the scattered field, $E_{sc}(x,z)$ and the incident field, $E_{inc}(x,z=0)$, where the incident field is the solution to the homogeneous wave equation. In this weak-scattering limit, the total field on the right hand side of Eq. (1) can be replaced with the incident field; the wave equation then simplifies to

$$\left(\nabla^2 + k_0^2 n_0^2\right) E_{sc}(x,z) = -2k_0^2 n_0 \delta n(x,z) E_{inc}(x,z). \tag{3}$$

Chen and Stamnes have found from simulations that the Born approximation is valid over values of δn and radii of index structures, a, for $a\delta n \le 0.08\lambda$ [25]. In this work, we use the Born approximation for all calculations and show through our experimental data that this approximation is valid for the range of index structures we measure.

In the forward scattering problem, the right hand side of Eq. (3) is a known quantity. Solutions to this differential equation show that the Fourier transform of the scattered electric field can be calculated from the convolution of the Fourier transform of the incident electric field and the Fourier transform of the index profile [26]:

$$E_{sc}(k_x, L) = i\frac{k_0^2 n_0}{k_z} E_{inc}(k_x, z=0) *_{k_x} \left[\delta n_{obj}(k_x, k_z - k)\right] \exp\left[-ik_z L\right], \tag{4}$$

where $E_{sc}(k_x, L)$ is the one dimensional Fourier transform of the scattered field measured at a distance, L, from the object, $E_{inc}(k_x, z = 0)$ is the one dimensional Fourier transform of the incident field, and k_x and k_z are the spatial frequency coordinates in Fourier space. The k_z values are defined in terms of the k_x coordinates and the spatial frequency of the incident wave, k, such that $k_z = (k^2 - k_x^2)^{1/2}$. The scattered field measurements are therefore taken on arcs of the k-sphere in Fourier space as shown in Fig. 1. These measurements of the scattered field at various incident angles are used to determine the Fourier transform of the index structure, which is then inverse Fourier transformed to find the index profile in real space.

Because this data is taken on an irregularly sampled grid, this inverse transform is accomplished using a discrete Fourier transform (DFT) as opposed to the more efficient fast Fourier transform (FFT). For a transform with N data points, a DFT requires N^2 computations while an FFT requires NlogN computations, so an FFT will be much faster. Another solution to this problem is interpolation onto a regular grid in the Fourier domain [27]. A more common method of solving the inverse problem is filtered backpropagation, using interpolation in real space, which is an extension of the filtered backprojection commonly used in computed tomography with x-rays [28]. Both methods were developed to speed up implementation of the backpropagation of scattered fields for large data arrays. As we will demonstrate in Sec. 4, small data arrays (~200 points) are sufficient for reconstruction, and so a DFT proves to be sufficiently fast for our calculations.

#86306 - $15.00 USD Received 9 Aug 2007; revised 5 Oct 2007; accepted 10 Oct 2007; published 12 Oct 2007

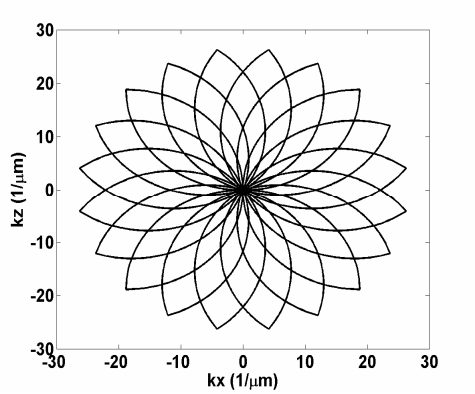

Fig. 1. Arcs in Fourier space representing the allowed propagating modes in the material at various incident electric field angles. The Fourier transform of the scattered field can only be measured along these arcs, resulting in an irregularly sampled grid of data.

A representative application of optical diffraction tomography is imaging deeply-buried waveguides, which are small in their physical dimensions and amplitude. Therefore, the diffracted field is typically smaller than experimental noise sources such as optical scatter, which can be significant when the small sample is embedded in a thick volume. To overcome this difficulty, consider an array of equally-spaced, identical index perturbations, such as an array of parallel waveguides, that form a grating with a diffraction efficiency that grows as the square of the number of illuminated lines. The total index change of all the lines, δn_{tot}, is the convolution of the index change of a single line, δn_{obj}, with a comb spaced at the grating period, Λ,

$$\delta n_{tot}(x,z) = \delta n_{obj}(x,z) *_x \mathrm{comb}(x), \tag{5}$$

where $*_x$ represents the one dimension convolution in x. The comb(x) and its Fourier transform, comb(k_x) are defined as

$$\begin{aligned} \mathrm{comb}(x) &= \sum_{n=-\infty}^{\infty} \delta(x - n\Lambda) \\ \frac{1}{\Lambda}\mathrm{comb}(k_x) &= \frac{1}{\Lambda}\sum_{m=-\infty}^{\infty} \delta\left(k_x - \frac{2\pi m}{\Lambda}\right) \end{aligned}. \tag{6}$$

For real experiments, finite-sized beams are used, and in many experiments these have Gaussian profiles. The incident field and corresponding Fourier transform are then given by:

$$\begin{aligned} E_{inc}(x) &= A_{inc}\exp\left[-\left(\frac{x}{w}\right)^2\right] \\ E_{inc}(k_x) &= A_{inc}\frac{w}{\sqrt{2}}\exp\left[-\left(k_x\frac{w}{2}\right)^2\right] \end{aligned}, \tag{7}$$

where A_{inc} is the amplitude of the Gaussian field, and w is the 1/e electric field radius. Using the expressions for the Fourier transform of the index perturbation and field in Eq. (4), we find

$$E_{sc}(k_x,L) = i\frac{k_0^2 n_0}{k_z}\frac{A_{inc}}{\sqrt{2}}\frac{w}{\Lambda}\exp\left[-\left(k_x\frac{w}{2}\right)^2\right] *_{k_x} \left[\delta n_{obj}(k_x, k_z - k)\mathrm{comb}(k_x)\right]\exp(-ik_z L). \tag{8}$$

This expression shows that in the far field, the diffracted electric field is given by the Fourier transform of a single index line sampled at a spatial frequency of one over the grating period.

#86306 - $15.00 USD Received 9 Aug 2007; revised 5 Oct 2007; accepted 10 Oct 2007; published 12 Oct 2007

The Gaussian incident field results in Gaussian shaped samples, or diffraction orders, in the far field, spaced at $2\pi/\Lambda$ in k_x as seen from the result of the convolution integral:

$$E_{sc}\left(k_x, L\right) = i\frac{k_0^2 n_0}{k_z}\frac{A_{inc}}{\sqrt{2}}\frac{w}{\Lambda}\exp\left[-ik_z L\right]\times \sum_{m=-\infty}^{\infty}\exp\left\{-\left[\left(k_x - \frac{2\pi m}{\Lambda}\right)\frac{w}{2}\right]^2\right\}\delta n_{obj}\left(\frac{2\pi m}{\Lambda}, k_z - k\right). \quad (9)$$

Because the power, and not the electric field, is measured at optical wavelengths, an expression for the Fourier transform of the index perturbation in terms of the power in each order of the diffraction grating is more useful. This is accomplished by taking the modulus square of Eq. (9) and then integrating over one grating period for each order of the diffraction grating. This gives an expression for the linear power in the m^{th} order of the diffraction grating in terms of the Fourier transform of the index perturbation at the particular value of k_x and k_z corresponding to that order:

$$\begin{aligned} P^m &= \int_{\left(m-\frac{1}{2}\right)\frac{2\pi}{\Lambda}}^{\left(m+\frac{1}{2}\right)\frac{2\pi}{\Lambda}} \left|E_{sc}\left(k_x, L\right)\right|^2 dk_x \\ &\approx \left(\frac{k_0^2 n_0}{k_z}\frac{A_{inc}}{\sqrt{2}}\frac{w}{\Lambda}\right)^2 \delta n_{obj}^2\left(m\frac{2\pi}{\Lambda}, k_z - k\right)\int_{-\infty}^{\infty}\exp\left\{-2\left[\left(k_x - \frac{2\pi m}{\Lambda}\right)\frac{w}{2}\right]^2\right\}dk_x \end{aligned}. \quad (10)$$

As long as the Gaussian beams well separated, the integral over a single order can be approximated as an integral over ∞ with very little error. The linear power in the m^{th} order is then given by:

$$P^m \approx \left(\frac{k_0^2 n_0}{k_z}\frac{1}{\Lambda}\right)^2 A_{inc}^2 w\sqrt{\frac{\pi}{2}}\delta n_{obj}^2\left(m\frac{2\pi}{\Lambda}, k_z - k\right). \quad (11)$$

The linear incident power is given by $(A_{inc})^2 w\sqrt{\pi/2}$. Now the Fourier transform of the index perturbation at $k_x = 2\pi m/\Lambda$ and the corresponding k_z value can be given in terms of the ratio of the scattered power measured in the far field and the incident power,

$$\delta n_{obj}\left(k_x = m\frac{2\pi}{\Lambda}, k_z - k\right) = \frac{k_z}{k_0^2 n_0}\Lambda\sqrt{\frac{P^m}{P_{inc}}}. \quad (12)$$

The Fourier transform of the index perturbation is now in terms of measurable quantities and can be calculated from power measurements of each order for a range of incident probe beam angles. The last step is to take an inverse Fourier transform, resulting in the quantitative, 2D cross section of the index perturbation.

The replication of the object results in a higher signal to noise ratio (SNR). The scattered field from each index line adds coherently, causing the peak intensity of the diffraction orders to grow as the square of the number of lines that are illuminated. While this does not increase the overall diffracted signal, the scattered signal is concentrated into a smaller area. By spatially filtering the signal so that only the diffracted order reaches the photodetector, uniform detected noise due to scatter is decreased, thus increasing the overall SNR. The width of the pinhole can be $2\pi/(2w)$, the width of the Fourier transform of the beam, while the samples are separated by $2\pi/\Lambda$. If the scatter noise is uniform, only $\Lambda/(2w)$ times the noise reaches the photodetector, while the entire signal is detected. This results in an increase of SNR of a factor of $(2w)/\Lambda$, or the number of lines of the grating that are illuminated by the

#86306 - $15.00 USD Received 9 Aug 2007; revised 5 Oct 2007; accepted 10 Oct 2007; published 12 Oct 2007

incident field. This can also be seen as decreasing the noise of the measurement system by averaging over many copies of the index perturbations in real space by recording only those Fourier components which correspond to the periodicity of the array. Since the peak intensity depends on the grating period for a fixed probe beam size, we can adapt to a wide variety of amplitudes of index changes by changing the period of the gratings.

The increased peak intensity at these discrete scattered orders comes at the expense of revealing only discrete samples of the object Fourier transform. As shown in Eq. (8), the convolution of the index structure in real space results in a sampling of the Fourier transform of the index perturbation. In the far field, the diffracted electric field is proportional to the Fourier transform of a single index line sampled at a spatial frequency, $dk_x = 2\pi / \Lambda$. The sampling of the Fourier transform defines the length, $L_x = 2\pi / dk_x = \Lambda$, in real space over which the index can be reconstructed. Therefore, the grating period is the maximum length in x over which the index can be reconstructed. If the grating period is significantly larger than the size of the feature to be imaged, measurement of these discrete diffracted orders is sufficient to reconstruct the index of a single object.

Replication of the index structures to be measured allows imaging of very weak structures, but accurate measurements using optical diffraction tomography are still difficult to implement in practice due to the requirement of phase information on the scattered electric field. Since the phase of the electric field can not be directly measured at optical frequencies, some form of phase reconstruction is required. Phase reconstruction usually requires measurements of the intensity of the scattered field at multiple planes, at least one of which is in the near field, or prior information about the object [29]. There are also methods that use holography or interferometric methods to measure the phase directly [30,31]. However, for index structures that are smoothly varying and symmetric, the Fourier transform of the perturbation is positive, real, and symmetric. Therefore, the diffracted electric field amplitude is given directly by the square root of the measured intensity and no phase reconstruction is necessary. This allows intensity measurements to be taken directly in the far field without a lens and does not require prior information about the index structure or interferometry.

3. Direct-write lithography

We use the direct-write lithography system described in [11] to write index structures in volume photopolymers using the perpendicular writing geometry shown in Fig. 2. For this system, as in many 3D lithography systems, the resulting index change will resemble the incident writing beam. Therefore, the index change created by dragging a Gaussian beam through the polymer will be symmetric and smoothly varying, thus fulfilling the requirements for optical diffraction tomography without phase reconstruction.

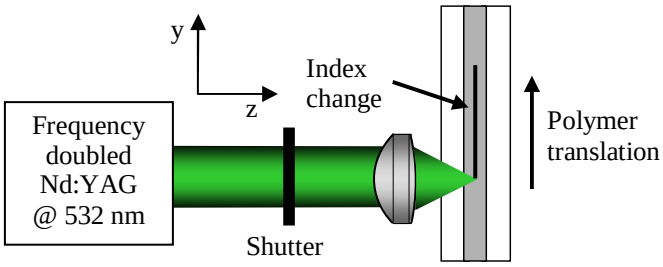

Fig. 2. Three-dimensional direct-write lithography system used for writing deeply-buried index structures in a volume photopolymer. The sample consists of 1 mm of photopolymer between two 1 mm thick pieces of glass. Green light is focused into the photopolymer with a molded asphere operating at 0.3 NA. The sample is moved perpendicular to the direction of propagation of the writing beam using high precision stages.

For all of the experiments described here, we use InPhase Technologies Tapestry™ HDS3000 media [1,32], which is sensitive to green light. The 7.6 x 7.6 cm square samples consist of 1 mm of photopolymer sandwiched between two 1-mm thick glass plates. A

#86306 - $15.00 USD Received 9 Aug 2007; revised 5 Oct 2007; accepted 10 Oct 2007; published 12 Oct 2007

frequency-doubled Nd:YAG laser at 532 nm is focused at a depth of 1.5 mm in the material with a 0.55 NA molded asphere corrected for spherical aberration due to 1.2 mm of glass. The system operates at 0.3 NA to avoid the need for active spherical aberration correction over the 1 mm polymer depth. We use high-precision stages to move the photopolymer in three dimensions. The diffraction gratings are optically ruled by focusing the green laser into the center of the photopolymer and translating the material in the *y* direction through the beam to draw a 5 mm line, with a constant change in index of refraction along *y*. A shutter is used to prevent the light from exposing the material in between the writing of each line. The writing powers for the data presented in this report range from 0.5–30 μW focused to a 0.75 μm $1/e^2$ radius. The size of the beam at the focus is measured using a razor blade knife scan. The speed of the stages during the writing process is 2 mm/s.

4. Optical diffraction tomography: experiment and results

The gratings measured in this experiment consist of 142 lines spaced 35 μm apart or 71 lines spaced 70 μm apart. Both configurations form 5 x 5 mm diffraction gratings. Once the gratings have been written and cured, we use a collimated 532 nm laser beam approximately 2 mm in diameter to measure the diffraction efficiency of the grating. The index structures written in the photopolymer have significant structure in the *z* dimension, but are thin in the sense of Bragg diffraction and therefore the scattered intensity has many diffracted orders in the *x* dimension in the far field. Each grating is rotated about the *y* axis to measure the efficiency of the diffracted orders versus incident angle, as shown in Fig. 3. A beam block is used to block light from all other orders and any scattered light. A high dynamic range power meter and filters measure four orders of magnitude in intensity, which corresponds to 10 or 20 diffracted orders depending on the size of the index structure and the period of the grating. Because the index is real, its Fourier transform is symmetric, so we only need to take data for positive values of k_x and k_z. Data is also taken only in the far field without the use of a lens, avoiding traditional field-of-view constraints.

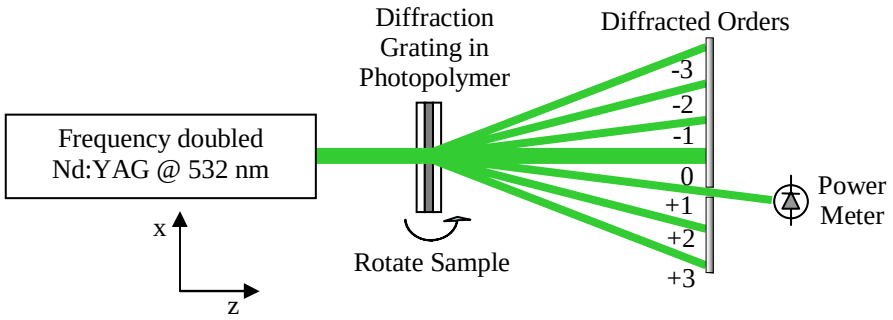

Fig. 3. Optical diffraction tomography experimental set up. Tomography measurements are taken after the samples are fully cured. A frequency-doubled Nd:YAG laser at 532 nm is used to probe the diffraction gratings. The sample is rotated to probe the grating at a variety of angles. Measurements are taken of each order at each angle with a high-dynamic-range power meter.

The diffraction efficiency data is processed using the method described in Sec. 2 and results in the reconstruction of the index of a single line in the *x*, *z* plane, as shown in Fig. 4. As expected, the cross section of the index qualitatively resembles the writing beam going through focus. Cross sections of this index are shown in Fig. 5. The cross section of δn in the *x* plane is taken at the center of the index in *z*, where $z = 0$. Similarly, the cross section of δn in the *z* plane is taken at $x = 0$. The ripples in the index reconstruction in *x* are caused by the finite sampling in Fourier space of the scattered field. For this data set, ten orders are measured for a grating with a period of 35 μm, corresponding to a maximum spatial frequency of $k_{x\,max} = 1.8\ \mu m^{-1}$, which gives a minimum sinusoidal period of 3.5 μm in the reconstruction as seen in Fig. 5(a). The noise on the data has an amplitude of approximately 2×10^{-4}. The

#86306 - $15.00 USD Received 9 Aug 2007; revised 5 Oct 2007; accepted 10 Oct 2007; published 12 Oct 2007

cross sections show that the index change in this photopolymer is not linearly proportional to the intensity of the focused writing beam, since the index shown is larger in scale than the *x*, *z* cross section of the writing beam.

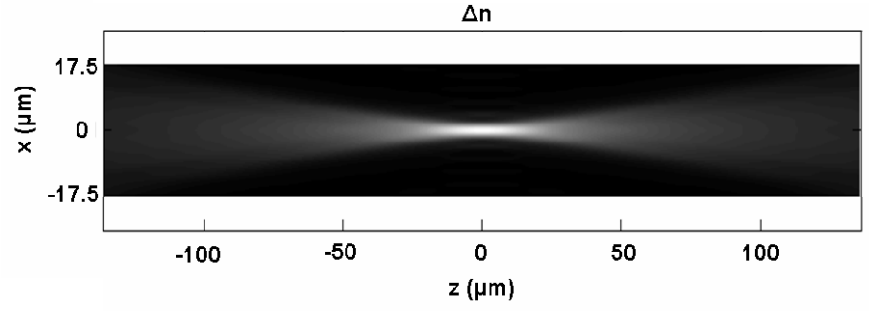

Fig. 4. Tomographic reconstruction of the cross section of the index of a single line of a diffraction grating written in photopolymer with the system shown in Fig. 2. The peak index change is 1.6 x 10^{-3}. Cross sections of the reconstructed index are shown in Fig. 5.

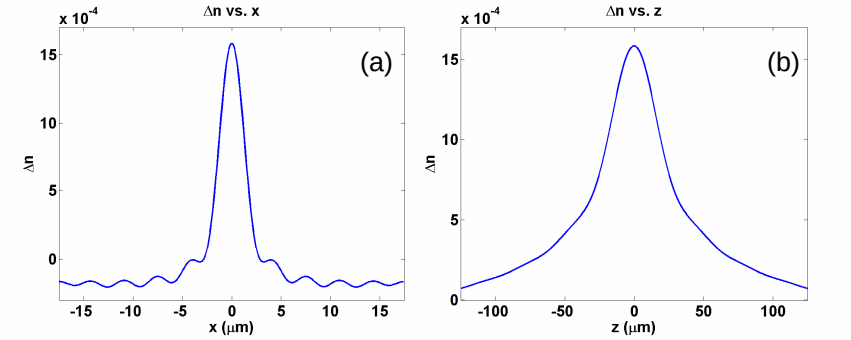

Fig. 5. Cross sections of the index change (shown in Fig. 4) written in the photopolymer in (a) x and (b) z at the peak of the index change. The cross section of δn in the x plane is taken at the center of the index in z, where z = 0. Similarly, the cross section of δn in the z plane is taken at x = 0. The small ripples of the index in the x cross section are due to the finite range of spatial frequency data supplied to the tomographic reconstruction algorithm.

In addition to having a high enough density of samples in Fourier space, a large enough range of spatial frequencies is also necessary for accurate reconstructions of the index. The range of spatial frequencies determines the resolution of the reconstruction. This is tested by removing samples from the highest spatial frequencies in k_x and k_z and observing the change in the full width at half maximum (FWHM) of the resulting index structures in *x* and *z*. As shown in Fig. 6, the FWHM's in both *x* and *z* approach a constant value as the number of samples is increased. Therefore, adding more samples, i.e. covering a larger range of spatial frequencies, will not significantly change the reconstructed index. Consequently, the reconstructed images are not limited by the resolution of the measurement system.

#86306 - $15.00 USD Received 9 Aug 2007; revised 5 Oct 2007; accepted 10 Oct 2007; published 12 Oct 2007

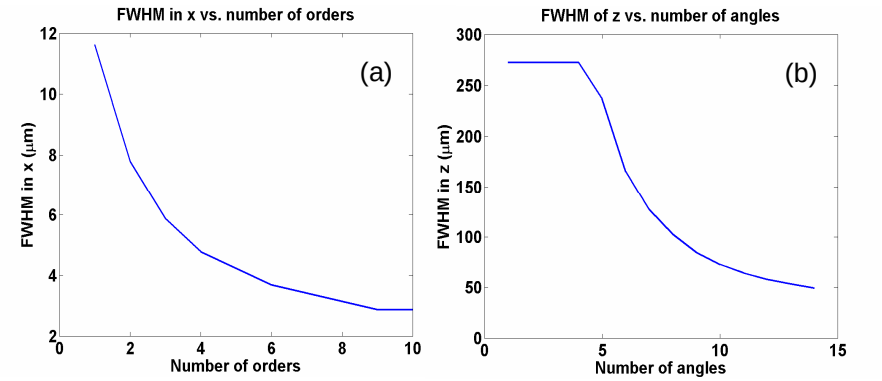

Fig. 6. Full-width at half-maximum (FWHM) measurements of cross sections of the reconstructed index as a function of data points used in the reconstruction algorithm. The slopes of both curves are approaching zero, indicating that additional samples will not change the feature size significantly.

The algorithm used in these reconstructions is based the Born approximation, and so it is also important to test whether the scattered field in this experiment obeys the Born approximation. An FFT beam propagation program simulates the forward scattering of a plane wave through the tomographic reconstruction of the index change without assuming the Born approximation. This tests the validity of the Born approximation for these experiments as well as testing for any errors in the reconstruction. The resulting calculated diffraction efficiency is shown in Fig. 7. The calculated efficiency is in good agreement with the experimental data, especially for the lower orders. To test the validity of the Born approximation, the efficiency is calculated for an index structure with a hundredfold lower amplitude. The resulting scattered field is multiplied by one hundred, and the intensity of this scattered field is compared with the experimental data. In this case, the agreement is much better for the higher orders. Scattering from weaker index structures would be closer in agreement with the Born approximation, but the error is still very small in our experiments. The FFT beam propagation simulation validates the magnitude and shape of the computed index as well as the use of the Born approximation for these index structures.

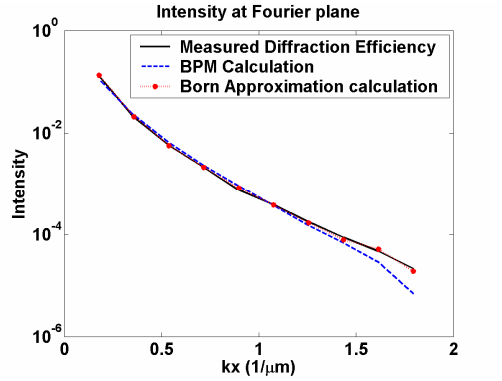

Fig. 7. Comparison of experimental diffraction efficiency and efficiency calculated from a fast-Fourier-transform beam-propagation method. There are no fit parameters used and so this calculation confirms both the shape and amplitude of the experimental reconstruction.

The tomographic image is also validated by comparing the reconstructed index with a qualitative image taken with a phase-shifted DIC microscope [33]. Because thin samples are ideal for imaging with DIC, the photopolymer sample is microtomed to a thickness of 10 μm. The sample is then covered with index matching fluid and a coverslip and imaged with a 10x, 0.3 NA objective [Fig. 8(a)] The phase-shifted DIC image does not directly show the index

#86306 - $15.00 USD Received 9 Aug 2007; revised 5 Oct 2007; accepted 10 Oct 2007; published 12 Oct 2007

profile, but is rather proportional to the change in the index profile along the *x* direction. To compare more directly, the tomographic reconstruction of the index is differentiated along the *x* direction and shown in Fig. 8(b). There is excellent agreement between the two images. There is also a much higher SNR for the tomography reconstruction due to the coherent addition of scattering from the individual index structures, giving a very clear image of the index change.

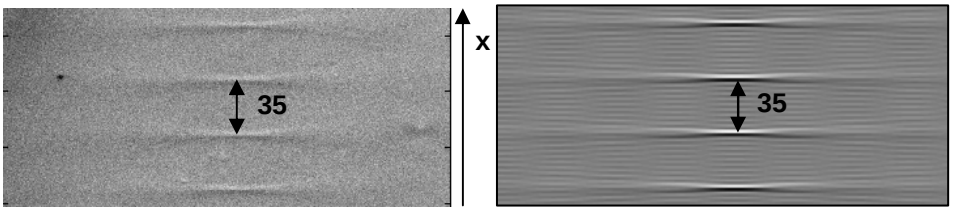

Fig. 8. Comparison of (a) phase-shifted Differential Interference Contrast image and (b) d/dx of an optical diffraction tomography reconstruction of a diffraction grating with a 35 μm period.

5. Conclusions

We have demonstrated quantitative measurements of deeply buried index structures in photopolymers. Our method of replicating a single weak index structure produces high-precision reconstructions of features as small as 3 μm by 150 μm with an index sensitivity of 2×10^{-4}. The transverse feature sizes are on the limit of the resolution allowed in the derivation of the expression for the index change in terms of scattered fields due to the approximation that the index is changing slowly on the order of a wavelength. For greater resolution, a more rigorous derivation without this approximation is necessary. The ability to change the period of the gratings also allows us to image a wide variety of index change amplitudes with good SNR. We have shown that for the class of smoothly varying, symmetric objects, optical diffraction tomography can be performed with intensity-only measurements, significantly simplifying the experiment and data analysis. We have fabricated many copies of index structures with the appropriate symmetries, reconstructed the index, and validated the reconstruction. A FFT beam propagation simulation is used to verify both the accuracy of the reconstruction and to provide a quantitative measure of the accuracy of the Born approximation. These images of weak index structures are essential for a variety of volume fabricated index structures where traditional microscopy cannot provide high-resolution, quantitative phase images.

Acknowledgments

This material is based upon work supported by the National Science Foundation under Grant Nos. (IIP-0637355, OII-05397731) as well an NSF-IGERT fellowship. The authors also acknowledge support from the Phillip Anthony Charitable Trust.

#86306 - $15.00 USD Received 9 Aug 2007; revised 5 Oct 2007; accepted 10 Oct 2007; published 12 Oct 2007